The Temperature-Composition Phase Diagram of Monomyristolein in Water: Equilibrium and Metastability Aspects

Jason Briggs and Martin Caffrey

Department of Chemistry, The Ohio State University, Columbus, Ohio, USA

ABSTRACT The temperature-composition phase diagram of monomyristolein in water was constructed using x-ray diffraction. Low- and wide-angle diffraction patterns were collected from samples of fixed hydration as a function of temperature in the heating direction on x-ray-sensitive film and/or image plates. The phases identified in the system include the lamellar crystalline phase, the lamellar liquid crystalline phase, the fluid isotropic phase, and two inverted cubic phases. Particular attention has been devoted to the issues of phase equilibrium and phase boundary verification.

Cubic phase undercooling was examined by adjusting the temperature of several samples in the cubic phase to a value where the lamellar liquid crystalline phase represents equilibrium behavior. Cooling-induced structure and phase changes were monitored continuously over a 30-min period by recording low-angle diffraction patterns from the samples using a streak camera. The cubic-to-lamellar transition rate decreased with increasing sample hydration. Additionally, the transition proceeded more rapidly at an incubation temperature of 25°C compared to that at 0°C. A mechanism is proposed that accounts for the hydration and temperature sensitivity of the phase transition under nonequilibrium conditions.

INTRODUCTION

Above certain limiting concentrations, amphiphilic lipid molecules aggregate when dispersed in water. These aggregates can access the liquid crystalline or mesophase state in a variety of ways. Several mesophases have been identified in lipid/water systems. These include the lamellar phases, where the lipid molecules assemble into stacked sheets; hexagonal phases, consisting of lipid/water cylinders packed on a hexagonal lattice; and three-dimensionally periodic phases that have cubic symmetry. This list is by no means complete, but it serves to introduce the variety of mesophases that are accessible in lipid/water systems.

The questions we wish to address in this research program take the following form: What is the relationship between the chemical structure of a lipid molecule and its liquid crystalline phase behavior? Why does one molecular species aggregate to form a lamellar phase under certain conditions while a closely related homologue forms a cubic phase under the same conditions? The work presented in this paper is part of a larger project aimed at answering these questions.

The relationship between molecular structure and phase behavior is being studied by comparing the temperature-composition (T-C) phase diagrams and the mesophase structure parameters for a homologous series of monoacylglycerols dispersed in water. A T-C diagram is a concise way of representing the equilibrium phase behavior of a system. The phase composition and relative amounts of coexisting phases at any temperature and overall composition can be determined from the corresponding T-C phase diagram. The lipid molecules under investigation consist of a series of cis-monounsaturated monoacylglycerols of varying chain length in the range of 14 to 22 carbon atoms. The single cis double bond is located at the 9 and 10 position of chains containing an even and odd number of carbon atoms, respectively. The T-C phase diagrams of the monoacylglycerol-in-water series will be determined using x-ray diffraction.

The series of phase diagrams, so generated, will provide a base of information from which certain aspects of the molecular structure-mesophase relationship can be established. These include identifying the equilibrium phases formed by each monoacylglycerol species under specific conditions of temperature and composition. Additionally, trends in the lattice parameters and thermal and compositional expansion coefficients of the different phases as a function of molecular structure will be established. In the spirit of the reductionist approach, the phase behavior of simple systems, such as the pure monoacylglycerols, must be understood before we come to appreciate the functioning of more complex lipid mixtures like those found in the biological membrane and in other lipid-rich aggregates such as atherosclerotic plaque, adipose tissue, lipoproteins, lung surfactant, and the stratum corneum. Models of lipid phase behavior derived from simple systems will provide a rational basis for selecting natural or synthetic lipid species that will exhibit desirable, user-defined phase characteristics with well-defined biochemical, medical, or industrial applications such as in the reconstitution of membrane proteins, the controlled release of encapsulated materials, or the formulation of substances with specific textures, organoleptic properties, and/or permeability characteristics.

Metastable behavior is often seen in hydrated lipid systems and can complicate the construction of a true equilibrium phase diagram. Instances of long-lived, nonequilibrium states can be mistaken for equilibrium behavior. Cubic

phases are notorious for their tendency to undercool, once accessed (Caffrey, 1987; Gruner et al., 1988; Lindblom and Rilfors, 1989; Mariani et al., 1988). However, even though metastable cubic phases can complicate the construction of a T-C phase diagram, in that they represent nonequilibrium states, they contribute valid and valuable information to the general understanding of the phase behavior of the system under investigation. Furthermore, there may be some aspect of the long-lived, undercooled phases that might be exploited. For example, Luzzati and co-workers suggest that the metastable character of cubic phases, formed by polar lipid extracts from the thermophilic archaebacteria *Sulfolobus solfactaricus*, is related to the rather harsh environments in which these organisms live (Mariani et al., 1988).

In this paper, the phase diagram of the first monoacylglycerol in the above series, namely monomyristolein (C14: 1c9), in water is presented. This lipid molecule contains a fatty acid chain 14 carbon atoms long with a *cis* double bond at the 9 position (Fig. 1). The chain is in ester linkage at the terminal hydroxyl of glycerol. X-ray diffraction was used to identify and characterize structurally the different mesophases found in the system in the temperature range of 0°C to 100°C and in the composition range of 0% (w/w) to 64% (w/w) water. Additionally, the results of an investigation into the phenomenon of cubic phase metastability is presented.

MATERIALS AND METHODS

Materials

Myristoleic acid was purchased from Nu Chek Prep Inc. (Elysian, MN) and was used without further purification. All other materials were of reagent grade. Water was purified by using a Milli-Q Reagent Water System (Millipore Corporation, Bedford, MA). This system consists of a carbon filter cartridge, two ion-exchange filter cartridges, and an organic removal cartridge.

Synthesis

Monomyristolein was prepared using a scaled-down version of the modification by Quinn et al. (1967) of the Hartman (1960) procedure. Benzene (55 ml) and p-toluenesulfonic acid (0.23 g) were added to a 100-ml round-bottomed flask containing glycerol (4.72 g), acetone (10 ml), and a few Teflon boiling chips. The flask was fitted with a Dean-Stark trap, a water-cooled condenser, and a drying tube containing Drierite (W. A. Hammond Drierite Company, Xenia, OH). The mixture was refluxed for 8 to 12 h, during which time approximately 1 ml of water was collected in the trap. This dehydration accompanied the formation of isopropylidene glycerol, which serves to protect two adjacent hydroxyl groups of glycerol from subsequent esterification. After cooling to room temperature, 5 g myristoleic acid was added, and the mixture was refluxed for 15 h as above. This step yielded an additional 0.4 ml water as a result of the esterification of the acid with the free hydroxyl group of the protected glycerol. After cooling to room temperature, anhydrous sodium acetate (0.3 g) was added to the flask fitted with the drying tube, and the mixture was swirled by hand for 10 min and washed four times with 10 ml water/wash to remove the p-toluenesulfonic acid and unreacted isopropylidene glycerol. The solvent was removed from the extracted material by rotary evaporation after drying for 10 min at room temperature over anhydrous sodium sulfate. The oily product was dissolved in 30 ml 2-methoxyethanol, to which 10 g boric acid was added. The round-bottomed flask, fitted with a room temperature air-cooled condenser and drying tube, was heated on a steam bath for 90 min to remove the protecting group. After cooling to room temperature, anhydrous diethyl ether (100 ml) was added, and the mixture was washed four times with 70 ml water/wash. The organic solvent was removed by rotary evaporation at room temperature after drying over anhydrous sodium sulfate for 10 min. The product had the appearance of a clear, light-yellow oil.

Purification

The entire product obtained from the synthesis above was dissolved in 60 ml hexane:diethyl ether, 9:1 by volume. Crystallization of monomyristolein was initiated by cooling the solution in a liquid nitrogen/chloroform slush for approximately 15 min. The bulk of the solvent was removed from the fluffy white crystals by filtering through qualitative grade filter paper (no. F2213-70; Baxter Healthcare Corporation, McGaw Park, IL) using a Buchner funnel at room temperature. After filtration, the "crystals" were transferred rapidly to a cold petri dish sitting in a pool of liquid nitrogen. This step was implemented to prevent the lipid from redissolving in the residual solvent by keeping the temperature low. The petri dish was transferred to a vacuum dessicator, and any remaining solvent was removed in vacuo for 6 to 12 h. Usually two crystallizations were required to obtain a product of >99% purity (as determined by thin-layer chromatography (TLC); see below). Product yield varied with each separate procedure. This is most likely due to crystals redissolving in the crystallizing solvent as the temperature increased during the room temperature filtration. Typically, 4 g of racemic monomyristolein was obtained from 5 g of the limiting reagent, myristoleic acid.

FIGURE 1   CPK space-filling model of monomyristolein. A length scale plus identifying features of the molecule are included.

Thin-layer chromatography

The purity of the synthesized product was determined by TLC. TLC plates (Adsorbosil-Plus Prekotes, no. 16385; Alltech, Deerfield, IL) were pre-run in a solvent mixture consisting of chloroform:methanol (10:1 by volume). Quantities of monomyristolein in chloroform were loaded onto the plate, giving spot sizes ranging from 1 to 500 μg lipid. The plate was developed in a solution of chloroform:acetone:methanol:acetic acid (73.5:25:1:0.5 by volume) (Jensen and Pitas, 1976) and visualized by charring on a hot plate (240°C) after spraying with Zinzadze reagent (Dittmer and Lester, 1964).
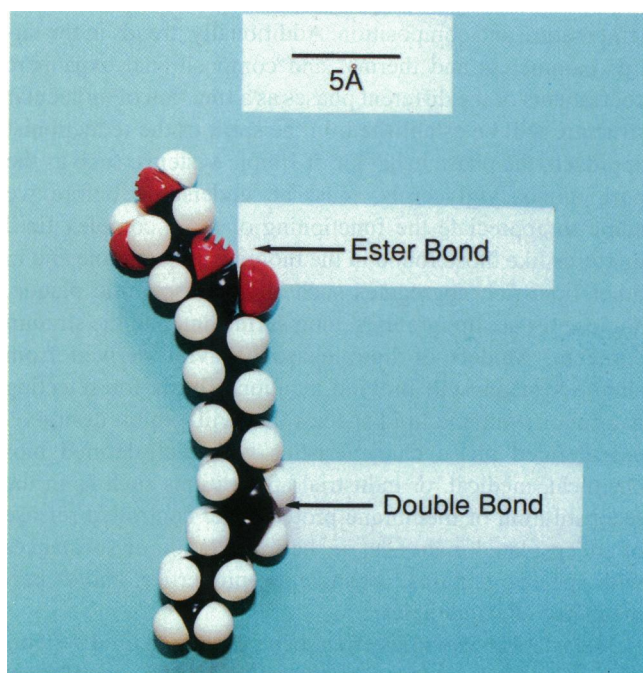
The Rf value of the lipid was 0.62. By comparing the intensity of the 1-μg spot to the impurities in the lanes corresponding to the 100-μg to 500-μg samples, the purity of the sample was determined to be $\geq 99\%$. One hundred-microgram spots were also developed in three other solvent systems and showed no trace of impurity (Jensen and Pitas, 1976). These solvent systems were (a) petroleum ether:diethyl ether:acetic acid (74:25:1 by volume) (Rf = 0.38), (b) petroleum ether:diethyl ether (94:6 by volume) (Rf = 0), and (c) chloroform:acetone (96:4 by volume) (Rf = 0.19).

Spectroscopic analysis

A proton nuclear magnetic resonance spectrum of the synthesized material was collected on a Bruker AM-250, 250 MHz machine at 27°C. Fifteen milligrams of lipid was dissolved in ~ 0.5 ml deuterated chloroform containing 0.03% (v/v) tetramethylsilane (Aldrich Chemical Company, Inc., Milwaukee, WI). Resonance peaks were assigned as outlined by Kates (1986). The general features of the spectrum compared favorably with that of monostearin, a saturated monoacylglycerol with a fatty acid 18 carbon atoms long (Kates, 1986). Peaks were identified in the monomyristolein spectrum at the chemical shift values indicated below, with the ratio of the experimental to the expected intensity of the peaks shown in parentheses. The glycerol methylene protons were observed at 3.6 to 4.3 ppm (3.9/5.0), the double bond protons at 5.32 ppm (1.8/2.0), the allylic methylene protons at 2.0 ppm (6.8/4.0), protons at the C2 and C3 positions of the chain at 2.33 ppm (2.0/2.0) and 1.62 ppm (2.0/2.0), respectively, the terminal methyl protons at 0.9 ppm (3.0/3.0), and the remaining aliphatic protons at 1.3 ppm (13.4/12.0). There was an intense resonance at 2.15 ppm (9.1/2.0) corresponding to the hydroxyl protons which was considerably more intense than expected for monomyristolein. The enhanced signal is most likely due to a small amount of water dissolved in the deuterated chloroform. Two sharp peaks at ~ 1.35 and 1.41 ppm were seen with a total intensity of 3.1. These protons as well as the high resonance intensity of the allylic protons have been assigned to impurities.

Sample preparation

Samples of fixed hydration were prepared by mechanically mixing appropriate amounts of lipid and water to achieve the desired overall sample composition. Mixing was accomplished by cycling the lipid/water mixture between two 250-μl gas-tight syringes (Hamilton Company, Reno, NV) through a short (6-mm) 22-gauge coupling needle with an internal diameter of 0.3 mm. The mixture was passed through the coupler 100 times at room temperature before being loaded into 3-cm-long, 1.0-mm-diameter quartz x-ray capillaries (Charles Supper, Natick, MA).

Transfer of the hydrated material with minimal water loss was accomplished by removing the coupler and attaching a standard 22-gauge needle to the syringe containing the sample followed by rapid delivery of the sample into the capillary. The capillaries were flame sealed and glued with 5 min epoxy (Hardman Inc., Belleville, NJ). The sealed capillaries were stored at 4°C for 2 to 4 weeks before data collection. The actual composition of the samples was determined by injecting a small amount of the hydrated material, usually 10 to 20 mg, from the syringe used to load the capillaries, into preweighed (~ 8 mg), pierced plastic bubbles cut from common bubble-wrap packing material. Weighings were carried out on a microbalance (no. M3P-000V001, 3 μg resolution; Sartorius, Bohemia, NY). The lipid-loaded bubbles were subsequently opened and dried over phosphorus pentoxide in a vacuum dessicator for approximately 12 h and reweighed. Water content was calculated from the difference between hydrated and dried samples. The use of the plastic bubbles was found to be advantageous in that the water loss during the first weighing was minimal. In contrast, open aluminum foil weighing boats were not satisfactory because of a rapid loss of water while weighing the wet samples.

X-ray diffraction

X-ray source

The x-ray data were collected on either the A-1 or F-1 lines at the Cornell High Energy Synchrotron Source (CHESS) or on the X9A line at the Na-

tional Synchrotron Light Source (NSLS), Brookhaven National Laboratory. At CHESS, the machine energy was usually 5.26 GeV with an electron (positron in the case of F1) beam current between 50 and 80 mA. The wiggler enhanced x-ray beam was focused with a bent, asymmetrically cut Si (111) crystal monochromator and a rhodium-coated silicon mirror before passing through a 0.3-mm collimator (Charles Supper, Natick, MA). The x-ray beam energy was 8.0 keV (1.55 Å) and 13.6 keV (0.92 Å) on the A-1 and F-1 lines, respectively, with a typical x-ray flux on the order of 10^{10} photons/s through a 0.3-mm collimator at either station. Exposure times varied from 10 s to 1 min, depending on the station and the state of the optics. At NSLS, the machine energy was 2.528 GeV, and the operating beam current was between 135 and 180 mA. The x-ray beam was focused with the second of a double bounce Si (111) crystal monochromator and a nickel-coated aluminum mirror. No collimation was used at NSLS because of the highly convergent nature of the beam. The x-ray beam energy was usually 8 keV (1.55 Å) with a flux on the order of 10^{11} photons/s on the sample. Typical exposure time was 20 s. The sample-to-film distances used ranged from 10 to 40 cm, depending on the spatial resolution required.

Sample holder

A temperature-controlled, multiple sample holder, based on the design of Wack and Webb (1989), was used to collect both static and streak diffraction patterns. This device holds up to seven samples in a beryllium cell that is in thermal contact with two thermoelectric (Peltier) devices (CP2-15-06L; Melcor, Trenton, NJ) via a copper block. The thermoelectric devices are powered by a bipolar temperature controller (Cambion Model 809-3000-01; Cambridge Thermionic Corporation, Cambridge, MA). A LabVIEW-based control program (National Instruments, Austin, TX) was written that provides isothermal temperature control and temperature ramping.

Temperature was measured by using a thermistor (YSI5K; Yellow Springs Instrument Co., Inc., Yellow Springs, OH) located in the copper block. The temperature uniformity of the beryllium cell, measured by a copper-constantan thermocouple (diameter 0.01 in; Omega Technologies Company, Stamford, CT) at different positions in the cell, was typically less than 0.5°C. The temperature stability of the sample holder was better than 0.1°C over a 1-h period. The in-sample temperature differed slightly from that measured by the thermistor. This difference is dependent on the temperature of a circulating water bath, which is used as a heat sink for the Peltier devices. When the temperature difference between the water bath and the sample holder is less than 25°C, as was the case for the current work, a difference of less than 0.5°C was measured between the copper block and the sample.

The samples were positioned in the x-ray beam, one at a time, by means of a remotely controlled stepping motor. In order to minimize radiation damage, the samples were translated continuously a distance of 2 to 4 mm in the x-ray beam back and forth along the length of the sample. This procedure has the added benefit of yielding better powder diffraction patterns from the cubic phases which, in the case of stationary samples, can give spotty patterns.

Static X-ray diffraction

Samples of monomyristolein, ranging from 0% (w/w) to 64% (w/w) water and contained in x-ray capillaries at 4°C, were placed in the multiple sample holder at 0°C. The samples were incubated for approximately 15 min at 0°C before the first diffraction pattern was collected. Samples containing less than 28% (w/w) water were incubated for 5 min at fixed temperatures ranging from 0°C to 100°C, in 10°C intervals, before collecting the diffraction patterns. Most of the remaining data were collected from samples subjected to a 10°C/h (0.17°C/min) temperature ramp. The ramp was stopped at 5°C intervals, and the diffraction patterns were collected after a 2-min equilibration. All measurements were made in the heating direction.

Diffraction patterns were collected on different recording media, including x-ray-sensitive film (DEF-5; Kodak, Rochester, NY) and image plates (Fuji HR-III; Stamford, CT and Kodak, Rochester, NY). In some cases, particularly at high energies where the x-ray attenuation by film is small, a single piece of film was placed in front of the image plate in order to

capture the patterns in both formats. A multiple frame/streak film device was used to collect the diffraction patterns. This device consists of a variable-width vertical slit behind which a film cassette is translated by means of a stepping motor. In these experiments, the slit was adjusted to a width of ~3.3 cm. A lead mask was placed in front of the slit, reducing its length to 9.5 cm. This allowed for the collection of 14 individual 3.3 × 9.5 cm² patterns, in two rows of seven, using a single 20 × 25 cm² cassette.

When image plates alone were used, each pattern was radially averaged over 100° using two pie-shaped sectors of 50° on opposite sides of the circular patterns. The 50° sectors were centered on the top and bottom of the diffraction patterns, where the beam focus is sharpest. When collected on film, the diameter of each diffraction ring was measured using a digitizing tablet and the distance measurement function of the Sigma Scan software package (Jandel Scientific, Corte Madera, CA). The data were then processed by means of a Pascal program to calculate a d-spacing for each diffraction ring and to index the patterns to one or more of the several cubic space groups. The lattice parameters reported represent averages of the lattice parameters calculated from the individual indexed reflections in a single pattern.

Time-resolved X-ray diffraction

Time-resolved X-ray diffraction (TRXRD) was used to monitor the kinetics and structure changes upon cooling the different cubic phases into the fully hydrated lamellar region of the phase diagram. The experiments were designed such that the effect of incubation temperature and sample composition on the cubic phase undercooling process could be examined. Samples containing 36% (w/w), 41% (w/w), 50% (w/w), and 58% (w/w) water were incubated individually in the sample holder, described above, at a temperature (65°C to 70°C) known to stabilize one of the cubic phases. The samples were then rapidly cooled to either 25°C or 0°C while monitoring continuously the temperature and the low-angle diffraction pattern using the streak camera. When used in the streak mode, the camera slit was adjusted to a width of 2 mm and a height of 35 cm, and the film/image plate was translated behind it at a constant rate of 8 mm/min by the stepping motor. The resulting streak pattern was used to identify and determine the lattice parameter of the different phases formed during the undercooling and relaxation processes.

Cubic phase calculations

Cubic phase boundary verification

The phase boundaries in the monomyristolein/water phase diagram were hand drawn. The boundary position was based solely on the identification of pure phase regions and regions of phase coexistence using x-ray diffraction measurements at discrete points in temperature-composition space. The position of these hand-drawn cubic phase boundaries was verified by employing the following equation, derived by modeling the cubic mesophases using the infinite periodic minimal surface approach (Turner et al., 1992):

$$\Phi_1 = 2A_0\left(\frac{l}{d}\right) + \frac{4\pi\chi}{3}\left(\frac{l}{d}\right)^3. \tag{1}$$

Equation 1 describes the relationship between the volume fraction of a cubic unit cell occupied by lipid Φ_1, the lipid length (or, more precisely, the average thickness of the lipid monolayer in the cubic phase) l, and the cubic lattice parameter d. A_0 is a unitless quantity that relates the surface area of the infinite periodic minimal surface describing the cubic phase to the lattice parameter of that phase. χ is the so-called Euler characteristic and is dependent on the space group of the cubic phase (Anderson et al., 1989). The values of A_0 and χ used for the cubic phases identified in this system are shown in Table 1. Details of how Eq. 1 was used to verify the location of the cubic phase boundaries are given below.

Analysis of an x-ray diffraction pattern of a cubic phase yields both the identity (space group and thus, A_0 and χ) of the cubic phase and its lattice parameter. The composition of a *pure* cubic phase equals the total sample

TABLE 1 Geometric constants used in calculating l and Φ_l in Eq. 1*

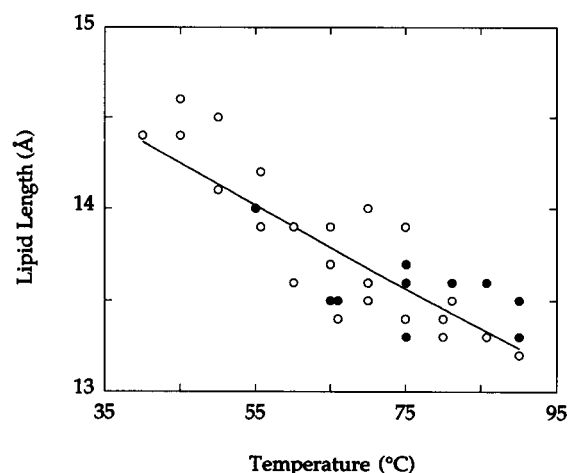| Cubic phase space group	A_0	χ
Ia3d	3.091	−8
Pn3m	1.919	−2

* Data from Anderson et al. (1989).

FIGURE 2 Temperature dependence of the lipid length, l, calculated for the pure cubic phases using Eq. 1. The data were fit with the following exponential relation: $l = 15.334e^{(-0.0016327)}$ where T is temperature in °C and l is in Å. The correlation coefficient was 0.84. Solid and open circles correspond to the Ia3d and Pn3m phases, respectively.

composition determined gravimetrically as described above. Assuming that the densities of the lipid and water in the cubic phase are the same, the weight fraction of lipid, obtained from the gravimetric measurement, is equal to the volume fraction of lipid in the cubic phase, Φ_1. Thus, for a pure cubic phase, both d and Φ_1 can be determined experimentally, and Eq. 1 can be solved for l. This procedure was repeated for every point in the phase diagram that corresponds to a pure cubic phase. The calculated values of l for the pure cubic phases are then used to determine the composition of cubic phases that are coexisting with a second phase (see below).

In this study, we found that there was no systematic dependence of l on cubic phase composition at a fixed temperature. With increasing hydration, the calculated value of l varied randomly within a narrow range. This variation is most likely due to error associated with measuring the lattice parameters of the cubic phases. The error range of l at any one temperature was rarely greater than 0.5 Å, however. The apparent insensitivity of l to both composition (Chung and Caffrey, 1994) and to phase identity has been noted previously (Turner et al., 1992). There is, however, a definite temperature dependence of l. Accordingly, the values of l calculated for the pure cubic phases were plotted against temperature in Fig. 2. The data were fit with the following exponential curve (correlation coefficient = 0.8402):

$$l = 15.334e^{(-0.0016327)}, \tag{2}$$

where T and l have units of °C and Å, respectively.

When a cubic phase coexists with some other phase, the composition of the individual coexisting phases cannot be determined easily without separating them physically. The approach that follows was used to determine cubic phase composition in such a situation. As with pure phases, x-ray diffraction measurements give the identity and lattice parameter, d, of the coexisting phases. Because l is insensitive to composition, Eq. 2 can be used to assign values of l to the cubic phases, regardless of their composition, at temperatures defined in or close to the temperature range upon which Eq. 2 is based. The composition of the cubic phase, coexisting with another

phase, was then determined by solving Eq. 1 for Φ_1 using the experimentally determined d and the assigned values of l. Φ_1 gives the composition of the cubic phase and, thus, the position of the cubic phase boundary at that particular temperature. In those cases where more than one diffraction measurement was made at a single temperature in a two-phase region, the calculated cubic phase compositions were averaged, and the mean value was taken as the position of the phase boundary at that temperature. This procedure was repeated for every point in the phase diagram that corresponds to a cubic phase in coexistence with a second phase, thereby allowing the hand-drawn and calculated cubic phase boundaries to be compared.

Undercooled cubic phases

Several hydrated lipid samples, at equilibrium in either the Ia3d or Pn3m cubic phase, were cooled to and incubated at a temperature that, under equilibrium conditions, should result in the formation of the fully hydrated lamellar liquid crystalline (L_α) phase. X-ray diffraction patterns were collected continuously during the cooling and low-temperature equilibration. The change in composition of the cubic phases with time during this process was calculated using Eq. 1. To this end, l was assigned to the cubic phases as above, using Eq. 2. However, in this case it was necessary to extrapolate to the appropriate undercooled temperature. The value of l, so assigned, was combined with the lattice parameter, d, determined from the streak pattern (above) and used to calculate the composition, Φ_1, of the undercooled cubic phases.

RESULTS

Temperature-composition phase diagram

The phases identified and their location in temperature-composition space are shown in Fig. 3. Fig. 4 *A* shows the phase boundaries and coexistence regions based on the static diffraction data in Fig. 3. The phases found in this system include the lamellar crystalline (L_c) phase, the L_α phase, the fluid isotropic (FI) phase, and two inverted cubic phases belonging to space groups Pn3m (Q^{224}) and Ia3d (Q^{230}). Between 0°C and 25°C an L_c phase is identified in dry lipid samples. This crystalline region may contain more than a single polymorph, but this aspect of dry monomyristolein behavior was not examined further. The L_c phase in the dry lipid converts to the FI phase at approximately 25°C. The L_α
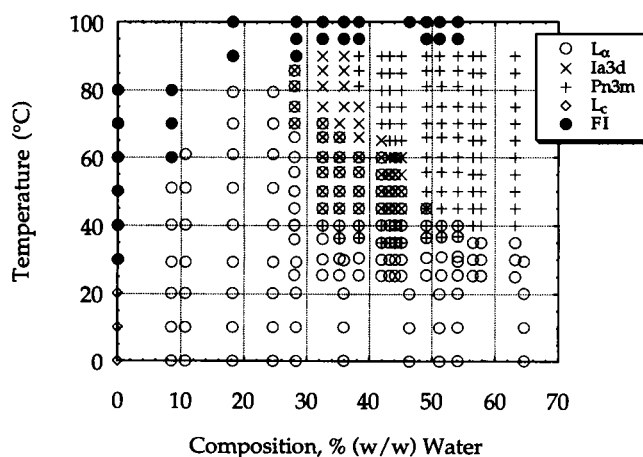

FIGURE 3   Identity and location in temperature-composition space of each phase in the monomyristolein/water system as determined by x-ray diffraction in the heating direction.
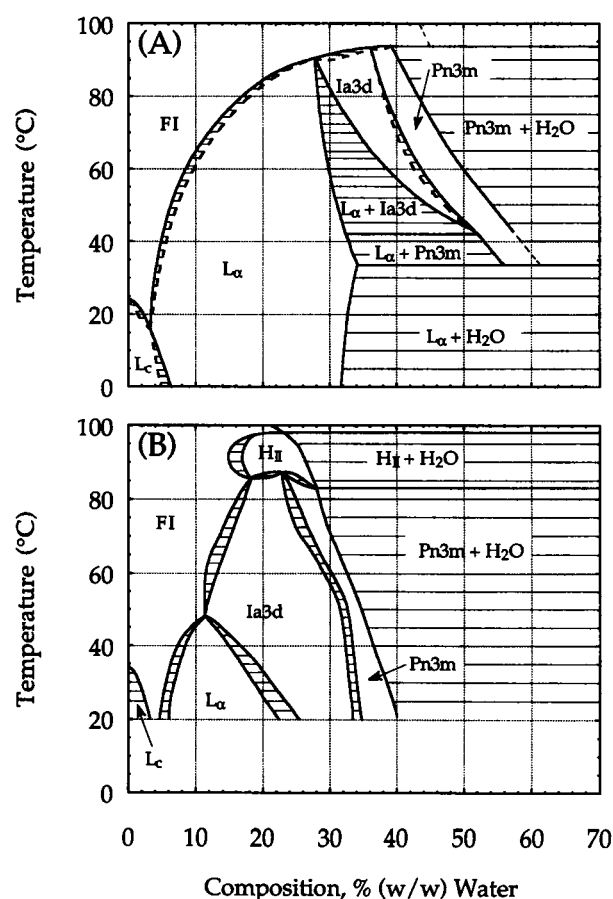

FIGURE 4   (*A*) Temperature-composition phase diagram of the monomyristolein/water system based on an interpretation of the data in Fig. 3. Boundaries indicated by dashed lines have not been experimentally verified and are so positioned to follow the Gibbs phase rule. (*B*) Temperature-composition phase diagram of the monoolein/water system (redrawn from Hyde et al., 1984).

phase exists as a pure phase between approximately 5% (w/w) and 33% (w/w) water below 35°C. Above this temperature, the pure L_α phase region is roughly triangular in shape, with the upper apex located at a temperature of ~90°C and a composition of 28% (w/w) water. At hydration levels greater than ~33% (w/w) water and at temperatures below 35°C, the fully hydrated L_α phase coexists with an excess water phase (Fig. 4 *A*). The L_α and Pn3m phases coexist in the composition range of ~34% (w/w) to 56% (w/w) water at 35°C. This coexistence is found in the hydration range of ~33% (w/w) to 53% (w/w) water at 40°C (Fig. 4 *A*). The hydration boundary of the Pn3m phase lies above 56% (w/w) water at 45°C and is close to 41% (w/w) water at 90°C (Fig. 4 *A*). The L_α and Ia3d phases coexist between roughly 32% and 52% (w/w) water above 40°C. This phase coexistence region has an upper temperature limit of 90°C (Fig. 4*A*). The pure Ia3d phase is found above 40°C sandwiched between the L_α + Ia3d coexistence region and the narrow Ia3d + Pn3m coexistence region. The FI phase is formed above 95°C in samples containing greater than 38% (w/w) water and extends to a limiting value of approximately 25°C for the dry lipid (Fig. 4 *A*).

Mesophase expansion coefficients

The temperature and composition dependence of the unit cell dimension of the different mesophases found in the phase diagram above are shown in Figs. 5 and 6, respectively. The lattice parameter of all liquid crystalline phases examined decreases with increasing temperature (Fig. 5). This can be quantified conveniently as a thermal expansion coefficient defined as

$$\alpha = (1/\eta)(\Delta\eta/\Delta T), \tag{3}$$

where $\Delta\eta/\Delta T$ is the slope of a straight line fit to the temperature dependence of the lattice parameters (Fig. 5), over a limited temperature range, and η is the lattice parameter of the phase calculated from the equation of the fitted line at a specific temperature, T. The pure L_α phase has an α-value of -2.25 kK^{-1} evaluated at 30°C and 11% (w/w) water ($\eta = 34.8$ Å).[1] For the pure Ia3d phase at 70°C, the α-value is -1.49 kK^{-1} in a sample containing 38% (w/w) water ($\eta = 126.5$ Å). The pure Pn3m phase has an α-value of -3.17 kK^{-1} at 70°C in a sample containing 45% (w/w) water ($\eta = 89.6$ Å). Unlike the L_α phase, the Ia3d and Pn3m phases exist as *pure* phases only over narrow isoplethal temperature ranges, resulting in a limited number of data points used to determine these values. Interestingly, the lattice parameter of the cubic phases has a dramatically increased temperature dependence

FIGURE 6 Composition dependence of the lattice parameters of the phases found in the monomyristolein/water system at selected sample temperatures. The identity of the phases is as follows: O, L_α; ×, Ia3d; +, Pn3m.

when in coexistence with a second phase. This increase in temperature sensitivity, as compared to the pure cubic phases, reflects the change in cubic phase composition with increasing temperature in a two-phase region (Discussion). For example, in the sample containing 36% (w/w) water, the "calculated" α-values for the Ia3d and Pn3m phases are -13.6 kK^{-1} ($\eta = 143.4$ Å) and -22.6 kK^{-1} ($\eta = 123.4$ Å) at 55°C and 37°C, respectively, when coexisting with the L_α phase. The α-values for the different phases, along with the parameters used in calculating the coefficients, are collected in Table 2.

The compositional expansion coefficient is defined as

$$\beta = (1/\eta)(\Delta\eta/\Delta W), \tag{4}$$

where $\Delta\eta/\Delta W$ is the slope of a straight line fit to the composition dependence of the lattice parameters of the different phases (Fig. 6) over a limited hydration range, and η is the lattice parameter of the phase calculated from the equation of the fitted line at a specific composition, W. The value of β calculated for the water-stressed L_α phase is 103 ppm^{-1} at 30°C and 18% (w/w) water ($\eta = 36.4$ Å).[2] Likewise, the pure Ia3d phase yields a β-value of 136 ppm^{-1} ($\eta = 120.2$ Å) at 75°C and 35% (w/w) water. The β-value of the pure Pn3m phase is 180 ppm^{-1} at 80°C and 40% (w/w) water ($\eta = 80.9$ Å). Again, the cubic phases exist as pure phases only over
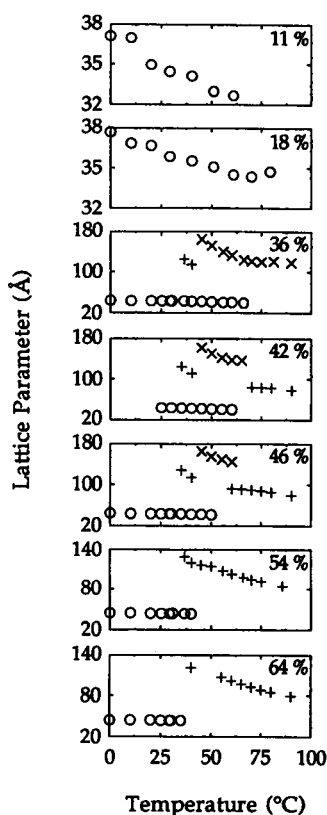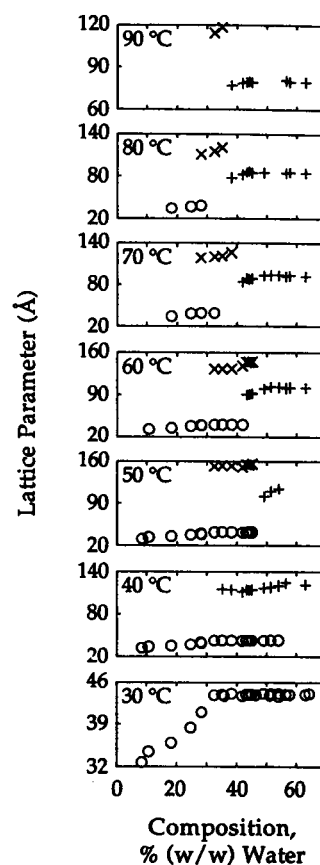

FIGURE 5 Temperature dependence of the lattice parameters of the phases found in the monomyristolein/water system at the indicated overall sample compositions in units of % (w/w) water. The identity of the phases is as follows: O, L_α; ×, Ia3d; +, Pn3m.

TABLE 2 Values of and parameters used in determining the thermal expansion coefficients of the different phases in the monomyristolein/water system

Phase	Sample composition, % (w/w) water	Temperature (°C)*	Equation of best fit[‡]	η (Å)[§]	α (kK^{-1})[¶]
L$_\alpha$ (pure)	11	30 (0–60)	$d = 37.1 - 0.0782T$ (0.9725)	34.8	−2.25
Ia3d (pure)	38	70 (65–75)	$d = 139.7 - 0.1889T$ (0.9956)	126.5	−1.49
Pn3m (pure)	45	70 (65–75)	$d = 109.5 - 0.2842T$ (0.9966)	89.6	−3.17
Ia3d (+L$_\alpha$)	36	55 (45–65)	$d = 250.8 - 1.9524T$ (0.9940)	143.4	−13.6
Pn3m (+L$_\alpha$)	36	37 (35–40)	$d = 226.8 - 2.7946T$ (1)	123.4	−22.6

* Temperature at which the thermal expansion coefficient was evaluated. The temperature range $(T_1–T_2)$ over which the temperature dependence of the lattice parameter was fit is indicated in parentheses.
‡ Equation of the straight line best describing the temperature dependence of the lattice parameter in the range indicated. The units of d and T are Å and °C, respectively. The correlation coefficient, R, of the fitted line is shown in parentheses.
§ η is the lattice parameter calculated at the temperature indicated used in determining the thermal expansion coefficient.
¶ The thermal expansion coefficient α is defined as $(1/\eta)(\Delta\eta/\Delta T)$, where $\Delta T = T_2 - T_1$ and kK^{-1} = kilo K^{-1}.

TABLE 3 Values of and parameters used in determining the compositional expansion coefficients of the different phases in the monomyristolein/water system

Phase	Temperature (°C)	Composition, % (w/w) water*	Equation of best fit[‡]	η (Å)[§]	β (ppm^{-1})[¶]
L$_\alpha$	30	18 (18–28)	$d = 29.7 + 0.3740W$ (0.9793)	36.4	103
Ia3d	75	35 (32–38)	$d = 62.8 + 1.6389W$ (0.9999)	120.2	136
Pn3m	80	40 (38–43)	$d = 22.8 + 1.4533W$ (0.9928)	80.9	180

* Sample composition at which the compositional expansion coefficient was evaluated. The composition range $(C_1–C_2)$ over which the composition dependence of the lattice parameter was fit is indicated in parentheses.
‡ Equation of the straight line best describing the composition dependence of the lattice parameter in the range indicated. The units of d and W are Å and percentage (w/w) water, respectively.
§ η is the lattice parameter calculated at the composition indicated used in determining the compositional expansion coefficient.
¶ The compositional expansion coefficient β is defined as $(1/\eta)(\Delta\eta/\Delta W)$, where $\Delta W = C_2 - C_1$ and ppm^{-1} is [parts per million (w/w) water]$^{-1}$.

a narrow range of hydration, giving a limited number of data points that can be used in determining these values. Table 3 presents a summary of β-values for the different phases, along with the parameters used in their calculation.

Boundary verification

The phase boundaries in the T-C phase diagram (Fig. 4 A) were hand drawn based solely on the identification of pure phase regions and regions of phase coexistence at specific temperatures and sample composition using x-ray diffraction. The positions of the boundaries, so drawn, were verified using Eq. 1 as described under Materials and Methods. Briefly, the lipid length, l, was calculated for the *pure* cubic phases using the lattice parameter, d, determined from diffraction measurements, and the known sample composition, Φ_l. The calculated values of l were plotted against temperature, and the corresponding data were fit with an exponential (Fig. 2). The latter was used to assign values of l to cubic phases *in a two-phase region* at a specific temperature. This assignment of l as a function of temperature is possible because lipid length is independent of composition at a fixed temperature (Chung and Caffrey, 1994; Turner et al., 1992). The assigned values of l, together with d values determined from x-ray diffraction measurements in the two-phase region, were used in Eq. 1 to determine the Φ_l value of the coexisting cubic phase. The calculated cubic phase composition gives the position of the cubic phase boundary at that

temperature. When more than one diffraction measurement was made along a single isotherm within a two-phase region, the mean calculated cubic phase composition is reported as the boundary position.

Table 4 shows the Pn3m phase composition calculated from each diffraction pattern collected along the 70°C isotherm. In the two-phase Pn3m + H$_2$O region at 70°C, the calculated composition of the cubic phase remains essentially constant at an average value of 46.4% (w/w). As expected, below the estimated excess water boundary line the gravimetrically determined and calculated cubic phase composition agree. The difference between the hand-drawn phase boundary at 47% (w/w) water (Fig. 4 A) and the corresponding calculated boundary position is 0.6% (w/w) water at this temperature. The estimated and calculated phase boundaries at all temperatures where a cubic phase was found to coexist with a second phase agreed to within ±1% (w/w) water (data not shown).

Cubic phase undercooling

As mentioned in the Introduction, cubic phases often exhibit metastable behavior that can complicate the identification of equilibrium states in hydrated lipid systems. Indeed, while constructing the T-C phase diagram of a homolog, mono-palmitolein (C16:1c9), we encountered long-lived under-cooled cubic phases, the appearance of which depended greatly on sample hydration and thermal history. This be-

TABLE 4 Comparison of known sample composition and that calculated for the Pn3m phase at 70°C*

Known overall sample composition, % (w/w) water‡	Calculated Pn3m phase composition, % (w/w) water	Composition difference, % (w/w) water
41.9	41.3	0.6
43.2	44.3	-1.1
44.1	43.6	0.5
45.1	44.3	0.8
49.1	46.4	2.7
51.4	46.8	4.6
54.1	46.8	7.3
56.5	46.0	10.5
57.8	46.4	11.4
63.2	46.0	17.2

* The dashed line marks the estimated hydration boundary of the Pn3m phase at ~47% (w/w) water based on the static diffraction data recorded at 70°C. The Pn3m lattice parameter does not increase with the addition of water to samples containing more than 47% (w/w) water, indicating full hydration (Fig. 6).
‡ Gravimetrically determined values.

havior is not unique to the monoacylglycerols but is found in other lipid systems as well (Gruner et al., 1988; Gulick et al., 1985; Seddon, 1990; Shyamsunder et al., 1988). We wished to characterize this complex behavior at the level of the effect of sample composition and incubation temperature. To this end, samples containing 36% (w/w), 41% (w/w), 50% (w/w), and 58% (w/w) water were prepared. The first sample was incubated at 70°C, and the last three samples at ~65°C before being cooled to either 0°C or 25°C. According to the phase diagram (Fig. 4 *A*), which we consider to represent equilibrium behavior, at hydrations greater than 32% (w/w) water and below 35°C a fully hydrated lamellar phase is found. Thus, any cubic phases seen at these low temperatures represent nonequilibrium behavior. This set of experiments allowed the exploration of the effects of sample hydration and final incubation temperature on the structural and kinetic aspects of the relaxation of undercooled cubic phases toward equilibrium. An example of the original streak film diffraction data collected on one member of this series is shown in Fig. 7. The different parameters, including temperature, unit cell dimension, and cubic phase composition, determined upon cooling the 50% (w/w) water sample to 0°C, are shown in Fig. 8. These same parameters for all of the undercooling experiments are collected in Table 5. Each experiment is treated separately below.

36% (w/w) water

In this first experiment, a sample with 36% (w/w) water was incubated in the pure Ia3d phase at 70°C for approximately 5 min. The sample temperature was then reduced to 25°C. Immediately following the temperature quench, there was an initial rapid increase in the Ia3d lattice from 125 Å to 184 Å, which was accompanied by the formation of a relatively large amount of L_α phase (Table 5). This unit cell expansion corresponds to a calculated increase in hydration of the Ia3d phase from 37% (w/w) to 52% (w/w) water (Materials and
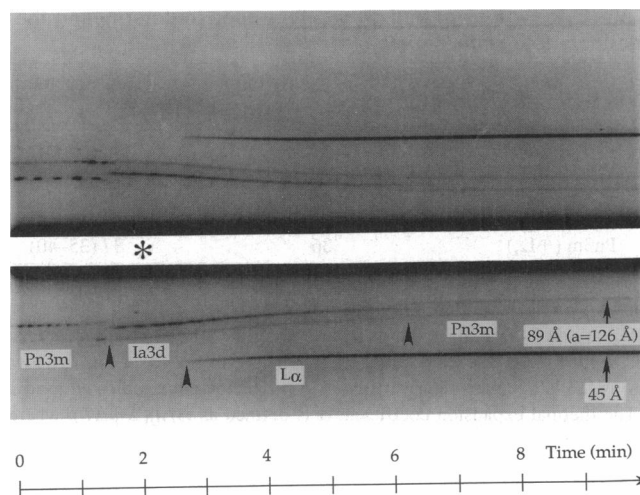

FIGURE 7 Portion of a streak low-angle x-ray diffraction pattern collected during cooling and low-temperature incubation of hydrated mono-myristolein initially in the Pn3m cubic mesophase. Sample composition was 50% (w/w) water. Temperature was jumped from 65°C to 0°C at *t* = 1 min. The film was translated behind a 2-mm slit at a constant rate of 8 mm/min. The sample-to-film distance was 709 mm. The x-ray wavelength was 0.895 Å. The identity of the different mesophases is indicated, and phase changes are marked with arrowheads. The d-spacing of the L_α (001) and Pn3m (110) reflections at an elapsed time of ~10 min is indicated. The corresponding cubic lattice parameter, *a*, is noted in parentheses. The horizontal axis corresponds to elapsed time and is so labeled. The vertical axis represents the scattering angle (2θ), with $2\theta = 0$ at and increasing in either direction above and below the asterisk. The white strip in the center of the streak film is where the beam stop blocks the direct beam. The dark band on either side of the white strip corresponds to leakage of the direct beam around the beam stop.

Methods). The newly formed L_α phase had a lamellar repeat spacing of 44 Å, which did not change with time during the course of the 23-min incubation at 25°C. Continued incubation to an elapsed time *t* of 2 min led to what appeared to be a replacement of the Ia3d phase, formerly coexisting with the L_α phase, by the Pn3m phase, which persisted for a 12-min period. The Pn3m lattice size expanded from 119 Å to 139 Å, while the relative amount of cubic phase in the system gradually decreased. This expansion of the Pn3m unit cell corresponds to an increase in cubic phase hydration from 54% (w/w) to 60% (w/w) water. After approximately 12 min at 25°C, the scattered x-ray intensity from the Pn3m phase was not discernible from background. Based on a close inspection of the streak film, an essentially pure lamellar phase remained at the end of the experiment.

Described above is the situation that prevails for a 70°C to 25°C quench. A similar behavior was observed when the final quench temperature was 0°C (Table 5).

41% (w/w) water

In this experiment, a sample containing 41% (w/w) water was cooled to 25°C after incubating in the Ia3d phase at 66°C. At the start of the experiment, the Ia3d lattice parameter was 135 Å, which corresponds to a calculated mesophase composition of 40% (w/w) water (Table 5). Upon cooling,
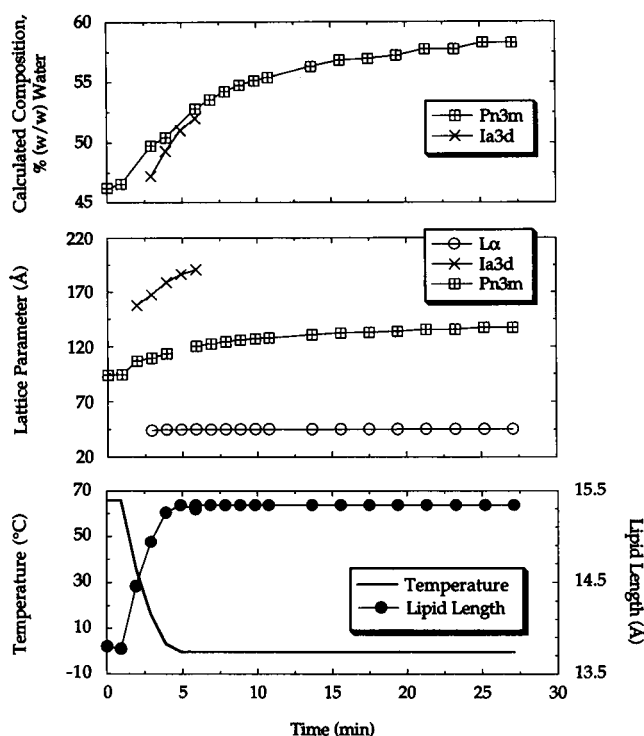
FIGURE 8   Time course of the different parameters measured and calculated during the Pn3m cubic phase undercooling experiment shown in Fig. 7. The parameters reported include sample holder temperature, lipid length in the cubic phases, lattice parameters, and calculated cubic phase composition.

there was an initial rapid expansion of the Ia3d lattice size to 182 Å accompanied by the formation of a large relative amount of L_α phase. The latter cubic lattice size yields a calculated Ia3d phase composition of 52% (w/w) water. As above, the lamellar repeat spacing of the coexisting L_α phase remained essentially constant at a value of ~44 Å for the duration of the 28-min experiment. Incubation at 25°C resulted in a relatively short-lived (1 min) three-phase coexistence of the L_α, Ia3d, and Pn3m phases beginning at $t = 3$ min. The newly formed Pn3m phase had an initial lattice parameter of 117 Å, which corresponds to a calculated composition of 54% (w/w) water. Continued incubation led to the disappearance of the Ia3d phase and to a coexistence of the L_α and Pn3m phases for the remainder of the experiment. At $t = 28$ min, the Pn3m lattice size was 136 Å, giving a final cubic phase composition of 60% (w/w) water.

Cooling from 66°C to 0°C yielded results similar to those reported above upon cooling to 25°C. The only notable difference was that the Pn3m phase appeared later ($t = 6$ min) and with a slightly larger initial lattice parameter of 122 Å, as opposed to 117 Å, in the sample with a final incubation temperature of 0°C (Table 5).

50% (w/w) water

A sample containing 50% (w/w) water was incubated in the Pn3m phase at 66°C before being cooled to 25°C (note that

in the previous experiments the starting cubic phase was of the Ia3d type). The Pn3m lattice parameter was 94 Å, which corresponds to a calculated cubic phase composition of 46% (w/w) water. At first glance this value might appear low when compared to the gravimetrically determined overall sample composition of 50% (w/w) water. However, as can be seen from the phase diagram in Fig. 4 A, the Pn3m phase coexists with an excess water phase under these conditions, and the composition of the cubic phase, as drawn, is approximately 47% (w/w) water.

Upon cooling to 25°C, the Pn3m lattice size increased slightly from 94 Å to 99 Å before converting to the Ia3d phase at $t = 2$ min (Table 5). The newly formed Ia3d phase had a lattice parameter of 158 Å. Incubation at 25°C resulted in the simultaneous expansion of the Ia3d lattice to 185 Å and formation of the L_α phase. This corresponds to an increase in Ia3d phase composition from 46% (w/w) to 53% (w/w) water. Continued incubation led to the disappearance of the Ia3d phase and to the coexistence of the L_α and Pn3m phases for the remainder of the experiment. The Pn3m lattice size increased from 117 Å to 136 Å after an elapsed time of 25 min. This corresponds to a change in hydration from 53% (w/w) to 60% (w/w) water. As was found in the previous undercooling experiments, the lamellar repeat spacing of the L_α phase remained virtually constant at a value of 44 Å during the course of the experiment.

When cooled from 66°C to 0°C, the Pn3m lattice size expanded from an initial value of 94 Å to 107 Å, whereupon most of the sample converted into the Ia3d phase at $t = 1$ min (Table 5). The newly formed Ia3d phase had a unit cell size of 158 Å, corresponding to a composition of 46% (w/w) water. Over a period of 5 min, the Ia3d lattice parameter increased to 191 Å with the gradual appearance of the L_α phase. This corresponds to an Ia3d phase composition of 52% (w/w) water. A barely detectable amount of the Pn3m phase coexisted with the Ia3d and L_α phases during this swelling process. The L_α phase had a lattice parameter of approximately 45 Å, which remained constant during the course of the 27-min experiment. Continued incubation at 0°C resulted in the conversion of the Ia3d phase back into the Pn3m phase. The Pn3m and L_α phases continued to coexist for the duration of the experiment with the cubic lattice increasing slowly from 120 Å to 137 Å. This corresponds to an increase in hydration of the cubic phase from 52.8% (w/w) to 58.3% (w/w) water (Fig. 8 and Table 5).

58% (w/w) water

In this experiment, a sample containing 58% (w/w) water was incubated in the fully hydrated Pn3m phase at 65°C before being cooled to 25°C. The Pn3m lattice parameter was initially 99 Å, giving a calculated cubic phase composition of 49% (w/w) water (Table 5). Quenching the sample to 25°C triggered the formation of the Ia3d phase at $t = 1$ min. At $t = 3$, the L_α phase appeared and coexisted with the Pn3m and Ia3d phases for several minutes. The Ia3d unit cell size increased gradually from 170 Å to 184 Å before disappearing

TABLE 5 Structure and composition parameters measured and calculated during the relaxation of undercooled cubic phases as a function of sample composition and incubation temperature following the imposition of a temperature jump*

Overall sample hydration	Temperature jump	Elapsed time (min)‡	Temperature (°C)§	Lipid length (Å)	Lattice parameter (Å)¶			Calculated composition % (w/w) water‖	
					L_α	Ia3d	Pn3m	Ia3d	Pn3m
36% (w/w)	70°C to 25°C	0	70.8	13.7	ND**	125.3	ND	36.9	ND
		1.5	50.8	14.1	44.1	153.1	ND	45.7	ND
		2.0	37.5	14.4	43.6	176.0	ND	51.2	ND
		2.5	26.2	14.7	44.1	184.1	118.6	52.4	54.0
		3.0	25.4	14.7	44.2	ND	121.0	ND	54.9
		15.6	25.3	14.7	44.5	ND	139.3	ND	60.5
		19.9	25.3	14.7	44.7	ND	ND	ND	ND
		23.3	25.3	14.7	44.7	ND	ND	ND	ND
	70°C to 0°C	0	70.7	13.7	ND	124.8	ND	36.7	ND
		1.5	53.0	14.1	42.0	128.1	ND	36.6	ND
		2.4	27.0	14.7	44.1	182.0	ND	51.9	ND
		2.9	18.1	14.9	44.1	ND	121.0	ND	54.3
		9.3	−0.4	15.3	45.0	ND	136.2	ND	58.1
		9.9	−0.4	15.3	45.2	ND	ND	ND	ND
		28.0	−0.4	15.3	45.2	ND	ND	ND	ND
41% (w/w)	65°C to 25°C	0	65.7	13.8	ND	135.3	ND	40.5	ND
		1.4	48.6	14.2	43.4	166.1	ND	49.2	ND
		2.4	25.6	14.7	43.8	176.9	ND	50.6	ND
		3.4	25.4	14.7	44.1	182.0	117.1	51.8	53.5
		4.4	25.4	14.7	44.2	184.1	118.6	52.3	54.0
		5.4	25.4	14.7	44.1	ND	120.0	ND	54.5
		28.1	25.4	14.7	44.7	ND	136.4	ND	59.7
	65°C to 0°C	0	65.8	13.8	ND	133.0	ND	39.6	ND
		2.0	37.3	14.4	43.2	161.5	ND	47.2	ND
		4.9	−0.4	15.3	44.9	186.0	ND	51.0	ND
		5.9	−0.4	15.3	44.9	188.0	122.2	51.5	53.6
		6.8	−0.4	15.3	44.9	189.6	122.3	51.9	53.6
		7.8	−0.4	15.3	44.9	ND	122.9	ND	53.8
		25.2	−0.4	15.3	45.0	ND	135.0	ND	57.7
50% (w/w)	65°C to 25°C	0	65.9	13.8	ND	ND	94.3	ND	46.5
		1.9	37.3	14.5	ND	158.5	99.4	46.2	46.9
		2.9	25.4	14.7	43.5	167.8	ND	48.1	ND
		4.9	25.4	14.7	43.9	181.5	ND	51.7	ND
		5.9	25.4	14.7	43.9	185.2	117.0	52.6	53.4
		6.9	25.4	14.7	44.2	ND	119.0	ND	54.1
		28.1	25.4	14.7	44.5	ND	136.3	ND	59.6
	65°C to 0°C	0	65.8	13.8	ND	ND	94.3	ND	46.6
		1.9	36.0	14.5	ND	157.8	106.7	45.9	50.2
		2.9	16.0	14.9	43.8	167.4	109.5	47.2	49.8
		3.9	3.0	15.3	44.5	178.8	113.5	49.3	50.4
		4.9	−0.4	15.3	44.7	186.5	ND	51.0	ND
		5.9	−0.4	15.3	44.9	190.6	120.3	52.0	52.8
		6.9	−0.4	15.3	44.7	ND	122.4	ND	53.6
		27.1	−0.4	15.3	45.2	ND	137.3	ND	58.3
58% (w/w)	65°C to 25°C	0	65.3	13.8	ND	ND	99.0	ND	48.8
		2.0	33.0	14.5	ND	169.5	110.3	49.2	51.4
		4.0	25.3	14.7	43.6	176.9	113.4	50.6	52.1
		7.8	25.3	14.7	44.2	184.1	116.9	52.4	53.4
		8.8	25.3	14.7	44.2	ND	117.6	ND	53.7
		28.0	25.3	14.7	44.7	ND	129.8	ND	57.8
	65°C to 0°C	0	65.7	13.8	ND	ND	98.1	ND	48.3
		1.9	34.5	14.5	ND	ND	114.9	ND	53.3
		5.8	−0.4	15.3	ND	ND	119.3	ND	52.5
		25.1	−0.4	15.3	ND	ND	131.1	ND	56.5

* X-ray diffraction data were collected continuously on streak film for the duration of the experiment. Entries are limited to the initial and final state of the system and to instances where a change in phase occurs.

‡ Elapsed time is referenced to a zero time when the x-ray shutter was opened and the diffraction measurement was initiated.

§ The temperature jump was initiated at an elapsed time of approximately 1 min (±10 s). The temperature reported is that of the sample holder block at the corresponding elapsed time.

¶ Lattice parameter is d_{001} for the L_α phase and a for the cubic phases.

‖ Calculated composition is based on the procedure described under Materials and Methods.

** ND indicates that the particular phase under consideration was not detected based on a close inspection of the streak film data.

after 4 min at 25°C. This corresponds to a change in Ia3d phase composition from 49% (w/w) to 52% (w/w) water. The L_α and Pn3m phases continued to coexist for the duration of the 28-min experiment, with the lamellar repeat spacing of the L_α phase remaining constant at 44.2 ($\pm$0.5) Å. The Pn3m lattice size increased to a final value of 130 Å, corresponding to a cubic phase composition of 58% (w/w) water. The relative amount of L_α phase formed in this experiment was considerably lower than in the less hydrated samples described above.

Cooling from an initial incubation temperature of 65°C to 0°C gave rise to an undercooled Pn3m phase, with no observable formation of either the Ia3d or L_α phases after 25 min. During the course of the experiment, the Pn3m lattice size gradually expanded from an initial value of 98 Å to 131 Å, corresponding to an increase in hydration from 48% (w/w) to 56% (w/w) water (Table 5).

DISCUSSION

Equilibrium phase behavior

One objective of this investigation was to construct the equilibrium temperature-composition phase diagram for the monomyristolein/water system. The question arises as to whether the diagram shown in Fig. 4 A represents true equilibrium phase behavior. If so, the phase diagram, as presented, should obey both the Gibbs phase rule and the lever rule, as described below.

The phase rule

The phase rule can be written in the following form (Gibbs, 1878):

$$C - P + 2 = F, \tag{5}$$

where F is the variance, C is the number of components in the system, and P is the number of phases coexisting under a particular set of conditions. This equation effectively limits the number of independent intensive variables while maintaining equilibrium between C components in P phases. The variables refer to pressure, temperature, and phase composition. The consequences of the phase rule, as applied to the monomyristolein/water system will be examined below.

Fig. 4 A represents a T-C phase diagram determined under conditions of fixed pressure. Thus, the phase rule for this system reduces to

$$C - P + 1 = F \tag{6}$$

and further to

$$3 - P = F \tag{7}$$

since monomyristolein in water is assumed to be a two-component system ($C = 2$). This simplified form of the phase rule (Eq. 7), where F includes only temperature and phase composition, is the rule that applies to the monomyristolein/water T-C phase diagram shown in Fig. 4 A.

The maximum number of phases that can exist in equilibrium with one another is determined by setting $F = 0$ in Eq. 7. Thus, no more than three phases can coexist in the monomyristolein/water system. In agreement with this consequence of the phase rule, there are at most three phases coexisting at any point in the phase diagram (Fig. 4 A). Also, when $F = 0$, neither the temperature nor the composition of the three coexisting phases is independently variable. Accordingly, all three phase regions in Fig. 4 A exist as discrete points such as the FI, L_α, and Ia3d triple point, or as horizontal lines separating two two-phase regions such as exists between the L_α + Ia3d and the L_α + Pn3m coexistence regions.

The very fact that three phase "regions" exist as lines rather than points in the T-C phase diagram suggests that the composition *can* be varied independently of temperature, in apparent violation of the phase rule. However, it is total sample composition and not the composition of the individual coexisting phases that is changing while moving along a three-phase isotherm. The relative amounts of the coexisting phases do change as sample hydration changes. Since $F = 0$, temperature must be invariant also. Thus, any three-phase line has, of necessity, zero slope and must be a true isotherm. This is consistent with the data presented in Fig. 4 A to within the resolution of our measurements.

The lever rule

Another test of equilibrium is adherence to the lever rule. The lever rule for the system at hand states that the relative amounts of two coexisting phases is equal to the relative lengths of the horizontal tie-lines that intersect the boundaries of the coexistence region in the phase diagram (Fig. 9). Furthermore, the *composition* of the coexisting phases is fixed along a single isotherm and is equal to the composition
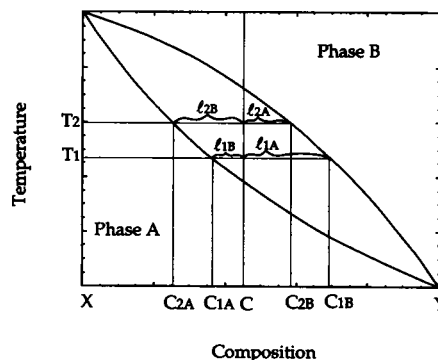

FIGURE 9 Demonstration of the lever rule in a hypothetical two-component phase diagram showing a lens-shaped phase coexistence with ideal mixing. At temperature T_1 and overall composition C, the composition of coexisting phases A and B is C_{1A} and C_{1B}, respectively. Under these same conditions, the relative amount of phase A is $l_{1A}/(l_{1A} + l_{1B})$, while that of phase B is $l_{1B}/(l_{1A} + l_{1B})$. At this same overall sample composition, increasing the temperature from T_1 to T_2 changes the composition of phase A from C_{1A} to C_{2A} and that of phase B from C_{1B} to C_{2B}. The relative amount of phases A and B at T_2 is $l_{2A}/(l_{2A} + l_{2B})$ and $l_{2B}/(l_{2A} + l_{2B})$, respectively.

corresponding to the points where the tie-lines intersect these boundaries. By way of an example, consider the 50°C isotherm in Fig. 4 A. As sample hydration is increased from 8% (w/w) to 28% (w/w) water, the lamellar repeat spacing of the *pure* L_α phase increases from 30 Å to 38 Å (Fig. 6). The increase in the lamellar repeat spacing suggests that the composition of the L_α phase is changing with sample hydration. Because this is a pure phase region, the lever rule does not apply. The L_α and Ia3d phases coexist in the range of 32% to 45% (w/w) water. Although there is a change in overall sample hydration in this composition range, the lattice parameters of the coexisting phases remain essentially constant at 42 Å and 152 Å for the L_α and Ia3d phases, respectively. These fixed lattice parameters suggest that the composition of the individual phases is remaining constant as the overall sample composition changes, in agreement with the lever rule. At 49% (w/w) water, a pure Pn3m phase emerges with a lattice parameter of 101 Å, which increases to 114 Å with the addition of more water in the single-phase region. Again, this is what is expected in a pure phase region. To within the resolution of our measurements, the lever rule is obeyed along every isotherm in Fig. 6.

Phase boundary slopes

The slope of the phase boundaries defining any two-phase region should reflect the temperature dependence of the composition of the coexisting phases. This concept is demonstrated schematically in Fig. 9. As the temperature is increased from T_1 to T_2, the composition of phase A changes from C_{1A} to C_{2A}, while that of phase B changes from C_{1B} to C_{2B}. If the slope of the boundary separating the single phase A from the two-phase region A + B is nearly vertical, the composition of phase A in the coexistence region is relatively temperature insensitive. As the slope of this boundary decreases, the composition of phase A in the coexistence region becomes increasingly temperature sensitive. Accordingly, the magnitude of the slope of the phase boundaries in Fig. 4 A, which were hand drawn based only on the identification of single- and two-phase coexistence regions by x-ray diffraction, should be reflected in the temperature dependence of the lattice parameter of coexisting phases. This is indeed the case, as will be illustrated by several examples from Fig. 5 as follows: (a) Heating the 36% (w/w) water sample from 0°C to 30°C, which remains fully hydrated in this temperature range, results in a 1 Å contraction of the lamellar lattice from 44 Å to 43 Å (Fig. 5). Following the simple reasoning outlined above, this suggests that the boundary separating the pure L_α phase from the fully hydrated L_α phase should be nearly vertical. Inspection of the phase diagram (Fig. 4 A) shows this to be the case. (b) The L_α and Pn3m phases coexist at 35°C and 40°C along the 36% (w/w) water isopleth. In this temperature range, the L_α lattice parameter remains constant at 43 Å, but the Pn3m lattice decreases from 125 Å to 115 Å with heating (Fig. 5). The fact that there is no change in the lamellar repeat spacing suggests that the L_α/L_α + Pn3m boundary should be close to vertical

between 35°C and 40°C, as is the case in Fig. 4. There is, however, a 10 Å decrease in the Pn3m lattice in this temperature range. Because the temperature sensitivity of the pure Pn3m phase lattice parameter is small (Table 2 and Fig. 5), this result suggests a fairly dramatic change in composition of the cubic phase upon heating through the coexistence region, giving a more gently sloped L_α + Pn3m/Pn3m boundary. This is exactly what is seen in the phase diagram (Fig. 4 A). (c) The L_α and Ia3d phases coexist in the temperature range from 42°C to 65°C at 36% (w/w) water (Fig. 4 A). The lamellar repeat spacing decreases slightly from 42 Å to 40 Å upon heating in this temperature range (Fig. 5). The small change in lamellar spacing again suggests a relatively constant L_α composition in this temperature range, and thus, the L_α/L_α + Ia3d boundary should be nearly vertical. In stark contrast, the Ia3d unit cell shrinks by 41 Å from 164 Å to 123 Å upon heating in the same temperature range. As was the case with the Pn3m phase above, this is consistent with a significant change in hydration of the cubic phase upon heating through the two-phase region due to the relatively insignificant temperature sensitivity of the lattice parameter of the pure Ia3d phase (Table 2). In turn, this suggests that the L_α + Ia3d boundary should be more gently sloped, as is found in Fig. 4 A.

Based on the evidence and arguments presented above, we submit that the phase diagram presented in Fig. 4 A represents equilibrium behavior. However, in hydrated lipid systems, metastable states can be accessed quite easily (Caffrey, 1987; Gruner et al., 1988; Lindblom and Rilfors, 1989; Mariani et al., 1988). In fact, equilibrium phase behavior is often much more difficult to establish than highly reproducible, nonequilibrium behavior. What, then, is the utility of a true equilibrium phase diagram? Is it not more useful to map out the most representative behavior of a system rather than a possibly more elusive equilibrium characteristic? Consider, for example, the different states of carbon. Under standard conditions, the thermodynamically favored state is graphite. The conversion of diamond to graphite is spontaneous but proceeds at an imperceptible rate. Thus, the saying "diamonds are forever" is not completely accurate. We remain speculative, however, as to the gratitude one might receive for giving the gift of graphite. The point of the digression is that, for a given set of conditions, there is one and only one equilibrium state for a system. There is no limit to the possible number of *non*equilibrium states that might be encountered under those same conditions. In this research program, we seek to compare the phase behavior of a homologous series of lipid molecules. It makes sense, therefore, to concentrate on the invariant equilibrium behavior.

Cubic phase undercooling

An investigation of the effect of incubation temperature and sample hydration on cubic phase undercooling and relaxation was conducted. Four samples of varying hydration were incubated at an elevated temperature that placed them in either the Ia3d or the Pn3m phase. The samples were then rapidly

cooled into the fully hydrated L_α region of the phase diagram. The temperature and low-angle diffraction patterns were collected continuously during cooling and low-temperature incubation. This allowed for an investigation of the structural and kinetic aspects of undercooled cubic phase relaxation. Some generalities concerning the undercooling behavior can be summarized as follows: (a) To some extent, the cubic phases experienced undercooling in all four samples. (b) The stability of the undercooled cubic phases increased with sample hydration in that a greater relative amount of undercooled cubic phase was present in the more hydrated samples at the end of each experiment (experiments lasted ~28 min). (c) The formation of the L_α phase occurred more rapidly at an incubation temperature of 25°C than at 0°C. (d) With one exception, there was an initial rapid increase in cubic phase unit cell size that was accompanied by the formation of a significant amount of the L_α phase. This rapid swelling of the undercooled cubic phase was followed by a period of more gradual swelling that continued for the duration of the experiment. A model consistent with these results follows.

Undercooling model

At any particular temperature, we hypothesize that there is a unit cell size that increases the stability of the undercooled cubic phase. Furthermore, as this unit cell size is approached, the lifetime for the metastable state is extended. Undercooling the cubic phase results in a dramatic increase in the size of the cubic unit cell (Fig. 8 and Table 5). Although a change in l contributes to this increase (Fig. 8), the large change observed in the cubic phase unit cell size during the course of the undercooling experiments is accounted for mainly by imbibition of water. If upon cooling, the cubic phase cannot access the desired lattice parameter, due to a limited supply of available water, the sample begins to convert from the undercooled cubic phase to the equilibrium L_α phase. However, if water is available or is made available to the metastable cubic phase, the desired lattice parameter can be approached.

According to the monomyristolein phase diagram (Fig. 4 A), the cubic-to-lamellar phase transition is a water-releasing event at overall sample compositions of greater than 32% (w/w) water. The water liberated upon the partial transformation of an undercooled cubic phase to the L_α phase can be taken up by any untransformed cubic phase, allowing it to swell. Depending on sample composition, different amounts of the L_α phase will be required to form such that the necessary water will be made available to the undercooled cubic phase. Consistent with this model we have found that cubic phase swelling was indeed observed to accompany the formation of the L_α phase in all but the most hydrated sample.

If a sample contains a large amount of excess water, an undercooled cubic phase can achieve the desired lattice parameter without the need for water to be released by the formation of a finite quantity of L_α phase. In contrast, with less hydrated samples, containing at least 32% (w/w) water,

there may not be sufficient free water available to allow the undercooled cubic phase to swell to its target lattice parameter. In this situation, the undercooled cubic phase will begin to convert to the L_α phase, releasing water that can be used to swell the remaining cubic phase. Support for this aspect of the model has been obtained in the cubic phase undercooling experiments as follows. In the sample containing 58% water, no L_α phase was formed upon cooling to 0°C, on the time scale of the experiment. Rather, the Pn3m phase undercooled as a pure phase. Obviously, there was enough free water available to the cubic phase in this sample such that no *extra* water, provided by the formation of L_α phase, was required to swell the cubic phase. However, in the sample containing only 36% (w/w) water, virtually all of the cubic phase was converted to the L_α phase before enough water was released to swell sufficiently the remaining undercooled cubic phase.

Another finding associated with the undercooling experiments was that the L_α phase formed more rapidly at an incubation temperature of 25°C than at 0°C. At the higher incubation temperature, more thermal energy is available to the system. This should increase the likelihood of moving out of any local energy minimum, corresponding to a metastable phase (Chvoj et al., 1991), and into the absolute energy minimum defining the equilibrium phase.

Comparison with other systems

The principal aim of this research program is to explore the relationship between molecular structure and mesophase behavior by comparing T-C phase diagrams for a series of homologous lipid molecules. Monoolein, C18:1c9, is one of the lipid molecules in the series for which the T-C phase diagram in the range of 20°C to 100°C is already available (Hyde et al., 1984). For purposes of comparison, this phase diagram has been redrawn and is shown in Fig. 4 B. The differences between the phase diagrams of monomyristolein (Fig. 4 A) and monoolein (Fig. 4 B) are quite dramatic. To begin with, shortening of the hydrocarbon chain by four methylene units, in going from monoolein to monomyristolein, results in the complete elimination of the H_{II} phase. In the monoolein system, this phase is seen as a pure phase at high temperatures, between ~87°C and 99°C, and in coexistence with excess water at hydration values above ~30% (w/w) water in the same approximate temperature range. The H_{II} phase is absent from the monomyristolein phase diagram. Thus, the Pn3m phase transforms directly into the FI phase upon heating fully hydrated monomyristolein. With monoolein, a fully hydrated Pn3m sample passes through the H_{II} phase upon heating and before melting to the FI phase.

A second consequence of chain shortening is a very pronounced increased stability of lamellar over cubic phases, as demonstrated by the following instances (compare Fig. 4, A and B): (a) In the monomyristolein system, the L_α phase is found at temperatures up to ~85°C. In the monoolein system, the L_α phase is not observed above 50°C. (b) Below 35°C, in the monomyristolein system, the L_α phase coexists

with an excess water phase. The Pn3m phase, on the other hand, is identified as the phase in equilibrium with excess water between ~20°C and 85°C in monoolein. (c) The cubic phases, especially the Ia3d phase, occupy a smaller region of temperature-composition space in the monomyristolein phase diagram than in that of monoolein.

The significant stabilization of the lamellar phase over cubic phases in the monomyristolein/water system agrees with molecular geometric packing arguments (Israelachvili, 1991). These define a so-called shape factor as $v/a_o l_c$, where v is the volume of the hydrocarbon chain(s), which is considered to be incompressible, l_c is the maximum effective hydrocarbon chain length, and a_o is the optimal surface area per molecule defined at the polar/nonpolar interface which minimizes the sum of energy contributions involved in packing individual amphiphilic molecules into bulk phases. As the value of the shape factor increases, there is an increasing tendency for the molecules to aggregate into structures with negative curvature such as the inverted cubic and H_{II} phase. Molecules having a dynamically averaged cone, wedge, or cylindrical shape tend to from spherical, cylindrical, and planar aggregates, respectively. The monoacylglycerols possess a relatively small polar head group when compared to that of the phospholipids (Fig. 1). In the former case, the volume occupied by the head group is quite small compared to that of the chain, giving the molecule an overall conical shape. Upon chain shortening, the average molecular shape is more cylindrical. Thus, the observed increased stability of the planar L_α phase in monomyristolein as compared to monoolein is supported by these arguments. This same type of behavior is observed when comparing the phase diagrams of the saturated homologs of monoolein and monomyristolein, namely monostearin (C18:0) and monomyristin (C14:0) (Lutton, 1965). In the former, the L_α and cubic phases occupy an approximately equal area of temperature-composition space, the L_α phase being stable at lower hydration levels and temperatures. In the monomyristin case, the L_α phase dominates the phase diagram, with the cubic phase(s) occupying only a small region at high temperatures and high sample hydration.

The phase diagrams of monomyristolein and monoolein (Fig. 4, A and B) also differ in the composition range in which the cubic and L_α phases coexist. In the monoolein phase diagram, the L_α + Ia3d phase coexistence region is narrow, ranging from ~22% (w/w) to 24% (w/w) water at 20°C. The corresponding region in monomyristolein is found in the range of 32% (w/w) to 52% (w/w) water at ~40°C. The Pn3m phase is not seen to coexist with the L_α phase in monoolein in the temperature range investigated (Hyde et al., 1984), but these two phases coexist in the composition range of ~35% (w/w) to 57% (w/w) water at 35°C in the case of monomyristolein.

A significant difference between the monomyristolein and monoolein systems lies in the position of the various hydration boundaries. With the exception of the L_α phase, which is fully hydrated at a composition of ~33% (w/w) water in the case of monomyristolein, full hydration occurs

at a higher water content in the monomyristolein system at any temperature in the range studied. For example, at 40°C, the limiting hydration value of the Pn3m phase is ~58% (w/w) water in monomyristolein. With monoolein, the corresponding value is ~36% (w/w) water. At 80°C, the Pn3m phase is fully hydrated at 44% (w/w) in monomyristolein. This phase is fully hydrated at a composition of 30% (w/w) water in monoolein at this temperature. At 90°C, the Pn3m phase is fully hydrated at 41% (w/w) water in the monomyristolein system. At this temperature in monoolein, the fully hydrated H_{II} phase is found with a composition of only 28% (w/w) water. The dramatic increase in the water-carrying capacity of monomyristolein, as compared to monoolein, may be related to the maximum lattice parameter that can be adopted by the nonlamellar phases, especially the cubic phases, in these systems. We can speculate that a larger-sized cubic phase unit cell is more stable in the shorter-chain lipid, increasing the water-carrying capacity of such materials. The ability to form cubic phases with large lattice parameters may result from the cylindrical shape of the monomyristolein molecule (discussed above) as follows. As the lattice parameter of a cubic phase increases, the environment experienced by each lipid molecule becomes increasingly planar, a morphology consistent with the molecule's more cylindrical shape. As x-ray data become available for the monoolein system, the correlation between water-carrying capacity and maximum cubic lattice parameter can be examined more fully.

Despite the differences, there are obvious similarities between the monomyristolein and monoolein phase diagrams. With the exception of the H_{II} phase, which is not present in the monomyristolein phase diagram, both systems exhibit the same phases in the same order with respect to temperature and hydration. At low hydration values and at low temperature, an L_c phase is found in both systems. The FI phase is formed directly from the dry material upon heating. Increasing sample hydration and temperature results in the formation of the L_α phase. The cubic phases are formed at higher hydration values. Additionally, the slopes of the boundaries separating the various phases have the same sign in both systems, although the magnitudes of the slopes are different. Interestingly, the upper temperature limit of the liquid crystalline phases is close to 100°C in both species.

CONCLUSION

In this paper the temperature-composition phase diagram of monomyristolein in water was presented. X-ray diffraction was used to identify and to structurally characterize the phases formed by monomyristolein in the temperature range of 0°C to 100°C and in the composition range of 0% to 64% (w/w) water. The phase diagram presented bears considerable resemblance to that of the longer-chain monoolein (Hyde et al., 1984). In both systems, a lamellar crystalline phase, the lamellar liquid crystalline phase, the fluid isotropic phase, and two cubic phases were found. However, the inverted hexagonal phase, present in the monoolein phase dia-

gram, is conspicuous by its absence from the monomyristolein phase diagram. In general, the lamellar phase is stabilized in the shorter-chain lipid. We note a dramatic difference in the water-carrying capacity between monomyristolein and monoolein. Specifically, the Pn3m phase of monomyristolein is fully hydrated at a composition of ~60% (w/w) water at 40°C. In monoolein, the maximum composition of this phase at the same temperature is 36% (w/w) water (Hyde et al., 1984). The structural basis for this large difference in hydration is currently under investigation.

Considerable effort was devoted to confirming that equilibrium phase behavior was represented in the phase diagram of the monomyristolein/water system. To this end, the Gibbs phase rule and the lever rule were used as indicators of equilibrium behavior. Based on this evaluation, the phase diagram, as presented, describes equilibrium behavior. In addition, a new procedure for the verification of cubic phase boundary locations was developed and implemented.

As cubic phase metastability is a common phenomenon in hydrated lipid systems, we attempted to identify conditions that might influence the metastable character of the cubic phases in this system. The degree of sample hydration was found to greatly affect the rate of equilibration of the undercooled cubic phase. A model was presented that is consistent with this result. A temperature dependence of equilibration rate was also identified.

REFERENCES

Anderson, D., H. Wennerstrom, and U. Olsson. 1989. Isotropic bicontinuous solutions in surfactant-solvent systems: the L_3 phase. *J. Phys. Chem.* 93:4243–4253.

Caffrey, M. 1987. Kinetics and mechanism of transitions involving the lamellar, cubic, inverted hexagonal, and fluid isotropic phases of hydrated monoacylglycerides monitored by time-resolved x-ray diffraction. *Biochemistry.* 26:6349–6363.

Chung, H., and M. Caffrey. 1994. The neutral area surface of the cubic mesophase: location and properties. *Biophys. J.* In press.

Chvoj, Z., J. Sestak, and A. Triska. 1991. Kinetic Phase Diagrams: Non-equilibrium Phase Transitions. Elsevier Science Publishers B.V., Amsterdam.

Dittmer, J., and R. Lester. 1964. A simple, specific spray for the detection of phospholipids on thin-layer chromatograms. *J. Lipid Res.* 5:126–127.

Gibbs, J. W. 1878. On the equilibrium of heterogeneous substances. *Trans. Conn. Acad. Sci.* 3:108–248.

Gruner, S., M. Tate, G. Kirk, P. So, D. Turner, D. Keane, C. Tilcock, and P. Cullis. 1988. X-ray diffraction study of the polymorphic behavior of *N*-methylated dioleoylphosphatidylethanolamine. *Biochemistry.* 27:2853–2866.

Gulick, A., V. Luzzati, M. De Rosa, and A. Gambacorta. 1985. Structure and polymorphism of bipolar isopranyl ether lipids from archaebacteria. *J. Mol. Biol.* 182:131–149.

Hartman, L. 1960. Preparation of α-monoglycerides by a modified isopropylidene-glycerol method. *Chem. Ind.* 55:711–712.

Hyde, S., S. Andersson, B. Ericsson, and K. Larsson. 1984. A cubic structure consisting of a lipid bilayer forming an infinite periodic minimum surface of the gyroid type in the glycerolmonooleat-water system. *Z. Kristallogr.* 168:213–219.

Israelachvili, J. 1991. Intermolecular and Surface Forces. Academic Press Inc., San Diego.

Jensen, R., and R. Pitas. 1976. Synthesis of some acylglycerols and phosphoglycerides. *Adv. Lipid Res.* 14:213–247.

Kates, M. 1986. Techniques of Lipidology: Isolation, Analysis and Identification of Lipids. Elsevier Science Publishers B.V., Amsterdam.

Lindblom, G., and L. Rilfors. 1989. Cubic phases and isotropic structures formed by membrane lipids-possible biological relevance. *Biochim. Biophys. Acta.* 988:221–256.

Lutton, E. S. 1965. Phase behavior of aqueous systems of monoglycerides. *J. Am. Oil Chem. Soc.* 42:1068–1070.

Mariani, P., V. Luzzati, and H. Delacroix. 1988. Cubic phases of lipid-containing systems. Structure analysis and biological implications. *J. Mol. Biol.* 204:165–189.

Quinn, J., J. Sampugna, and R. Jensen. 1967. Synthesis of 100-gram quantities of highly purified mixed acid triglycerides. *J. Am. Oil Chem. Soc.* 44:439–442.

Seddon, J. 1990. Structure of the inverted hexagonal (H_{II}) phase, and non-lamellar phase transitions of lipids. *Biochim. Biophys. Acta.* 1031:1–69.

Shyamsunder, E., S. Gruner, M. Tate, D. Turner, P. So, and C. Tilcock. 1988. Observation of inverted cubic phase in hydrated dioleoylphosphatidylethanolamine membranes. *Biochemistry.* 27:2332–2336.

Turner, D., Z-G. Wang, S. Gruner, D. Mannock, and R. McElhaney. 1992. Structural study of the inverted cubic phases of di-dodecylalkyl-β-D-glucopyranosyl-*rac*-glycerol. *J. Phys. II France.* 2:2039–2063.

Wack, D., and W. Webb. 1989. Synchrotron x-ray study of the modulated lamellar phase $P_{\beta'}$ in the lecithin-water system. *Phys. Rev. A.* 40:2712–2730.